



OPEN Investigation of the mechanical frequency response of ovine renal tissue at low frequencies

Faezeh Azimi Pirsoltan & Mohammad Reza Karafi

This study explores the mechanical properties of ovine renal tissue, focusing on resonance patterns at low frequencies. Using a universal tensile/compression testing machine, we examined the stress-strain behavior of the tissue under compression, revealing its non-linear viscoelastic characteristics. Dynamic Mechanical Analysis (DMA) and a dynamic shear rheometer were employed to measure the storage and loss moduli across various frequencies (0.01–10 Hz). The shear storage modulus ranged from 1 kPa to 48 kPa in the strain level of 0.5%, while the shear loss modulus varied between 2 kPa and 4 kPa. Experimental results showed no resonant behavior in the mechanical properties, including storage modulus, loss modulus, and tan delta, in both tensile and shear modes at frequencies below 10 Hz. A vibration test was conducted using a shaker to investigate the Frequency Response Function (FRF) of the kidney over the studied frequency range. The vibration tests revealed mechanical resonance in the kidney at approximately 3 Hz. A numerical modal analysis, conducted using COMSOL software, identified a natural frequency around 3 Hz, closely aligning with experimental observations. These findings suggest significant implications for understanding renal mechanics and developing medical applications.

Keywords Frequency response, Mechanical properties, Renal tissue, Resonance

The mechanical properties of biological tissues are crucial for understanding their functionality and response to external forces. Tissue stiffness is influenced by factors such as material composition, structure, and spatial distribution. Due to their complex and anisotropic nature, biological tissues exhibit mechanical behaviors that vary across different length scales and loading conditions¹. Understanding these properties is essential for biomedical applications, including disease diagnosis, noninvasive imaging, and artificial tissue development. For instance, empirical data on soft tissue mechanics are vital for enhancing medical simulations, such as laparoscopic surgery trainers that provide realistic haptic feedback based on intra-abdominal organ behavior^{2,3}. Additionally, mechanical characterization improves diagnostic accuracy^{4,5}, advances noninvasive imaging techniques⁶, and aids in designing artificial tissues for medical applications⁷. Various methodologies have been utilized to characterize tissue properties in vivo, ex vivo, or using tissue-mimicking materials. Among these approaches, the first-order Ogden hyper elastic model is frequently employed to estimate material properties, while indentation tests effectively characterize the compressive behavior of soft tissues under varying loading conditions⁸. Computational modeling further enhances our understanding of tissue mechanics, offering both quantitative and qualitative insights. Researchers have modeled the mechanical and structural properties of biological tissues, including renal tissue, to analyze their functional interactions⁹. Furthermore, studies have investigated the correlation between applied forces and the electrical properties of soft tissues, employing piezoresistive models and Finite Element Modeling (FEM) to predict mechanical-electrical behavior¹⁰. The integration of deep neural networks (DNNs) also represents a contemporary approach to overcoming the limitations of traditional constitutive models, enabling more accurate predictions of tissue elasticity in finite element simulations¹¹. To evaluate mechanical properties, a variety of testing methodologies have been applied, including Dynamic Mechanical Thermal Analysis (DMTA)¹², universal testing^{13,14}, rheometer testing^{15,16}, and Frequency Response Function (FRF) testing^{17,18}. These techniques provide valuable insights into the viscoelastic and structural behavior of soft tissues, particularly renal tissue. Given that kidneys frequently endure traumatic impact forces, diagnosing internal bleeding can be challenging¹⁹. Despite this, limited research has focused on their mechanical properties, with most existing studies relying primarily on ultrasound-based assessments. Techniques such as Viscoelastic Response (VisR) ultrasound have been employed to evaluate renal viscoelasticity, providing indirect measurements of tissue viscosity that assist in detecting conditions such as fibrosis and inflammation^{20,21}.

Faculty of Mechanical Engineering, Tarbiat Modares University, Tehran, Iran. email: karafi@modares.ac.ir

This study investigates the resonance patterns in the mechanical properties of ovine renal tissue at low frequencies and their implications for biomedical applications. To achieve this, a universal mechanical tensile/compression testing machine was used to generate stress-strain diagrams under compressive forces. Additionally, Dynamic Mechanical Analysis (DMTA) and a dynamic shear rheometer were used to assess mechanical properties at various frequencies. A vibration test was conducted using a shaker to analyze the Frequency Response Function (FRF) of the kidney across the frequency range under investigation. The experimentally obtained mechanical properties were then used to develop a numerical kidney model in COMSOL software for modal analysis, with the numerical results compared to the experimental findings.

Material and method

The kidneys are paired retroperitoneal organs responsible for filtering blood and regulating the ionic balance of extracellular fluid. Each kidney comprises modular units known as nephrons, which consist of a glomerulus for filtration and a tubular system that reabsorbs water and solutes while facilitating the secretion of waste. The structure of the mammalian kidney is best exemplified by the unipapillary form, commonly found in smaller species. This structure features a cortex that encases a pyramid-shaped medulla extending into the renal pelvis. The medulla is divided into outer and inner sections, with the outer medulla further divided into two distinct stripes^{22,23}. In this section, we present the results of mechanical compressive tests, Dynamic Mechanical Analysis (DMA), and dynamic shear rheometric tests conducted on the primary areas of the kidney. Finally, a vibration test of the whole organ using a shaker is employed to investigate the Frequency Response Function (FRF) of the kidney across the analyzed range of frequencies.

Mechanical compressive test

Fresh ovine kidneys ($N=6$) were obtained from male sheep (~2 years old) at a licensed slaughterhouse. The animals were not sacrificed specifically for this study. Tissues were collected immediately after routine slaughter under veterinary supervision, stored at ~0 °C, and processed on the same day. The study was approved by the institutional ethics committee of Tarbiat Modares University (Code: IR.MODARES.AEC.1402.055) and is reported in accordance with the ARRIVE guidelines. Cylindrical samples each diameter approximately 15 mm, height 4 mm, as shown in Fig. 1, are surgically removed from the kidney's cortex, and medulla regions. The surgery was performed at approximately 0 degrees Celsius.

Compressive stress ($\sigma = F/A$, F is normal force and A is area. A precise determination of the sample area was achieved using digital imaging and image processing methods. High-resolution images were analyzed, and the area was calculated through calibrated software to ensure accuracy and reproducibility. Compressive strain is the fractional decrease in length of an object ($\epsilon = \Delta l/l_0 + 0.5(\Delta l/l_0)^2$, Δl is change in length, l_0 is original length) due to a compressive stress. Young's modulus or elastic modulus is the ratio of stress to strain. The device used in this research is the Zwick/Roell Z050 Universal Testing Machine. The servo motor installed on this device can provide a moving speed of 0.001 to 2000 mm per minute.

Stress-strain curves of the cortex, medulla at different strain rates is shown in Figs. 2 and 3.

Based on Figs. 2 and 3, it is found that regardless of the different strain rates (5, 25, and 50 mm/min), the "toe region" is about 30% on all main areas of the kidney (cortex and medulla). The graphs indicate that none of these tissues exhibit a linear elastic region. A compressive test for the entire organ was conducted at three levels of strain rate. Figure 4 shows the kidneys for the compressive test. The results of this test are shown in Fig. 5.

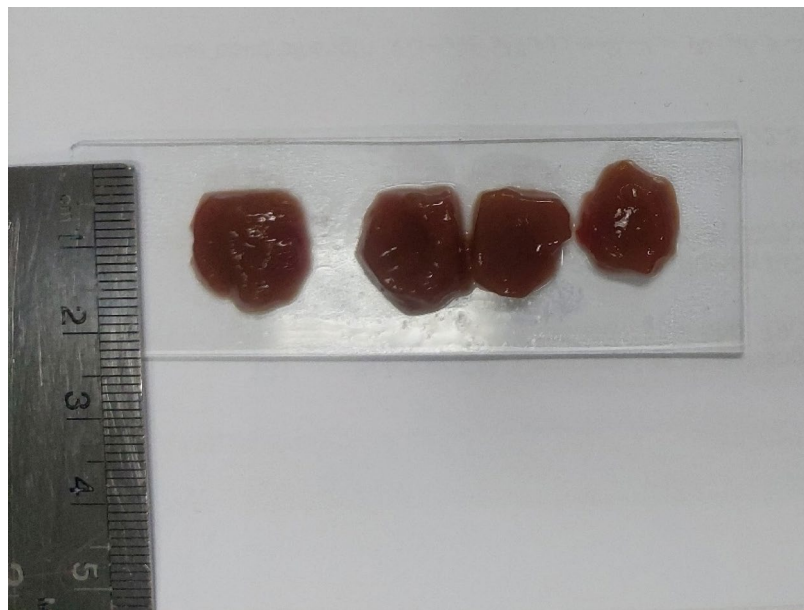


Fig. 1. Samples preparation for compression test.

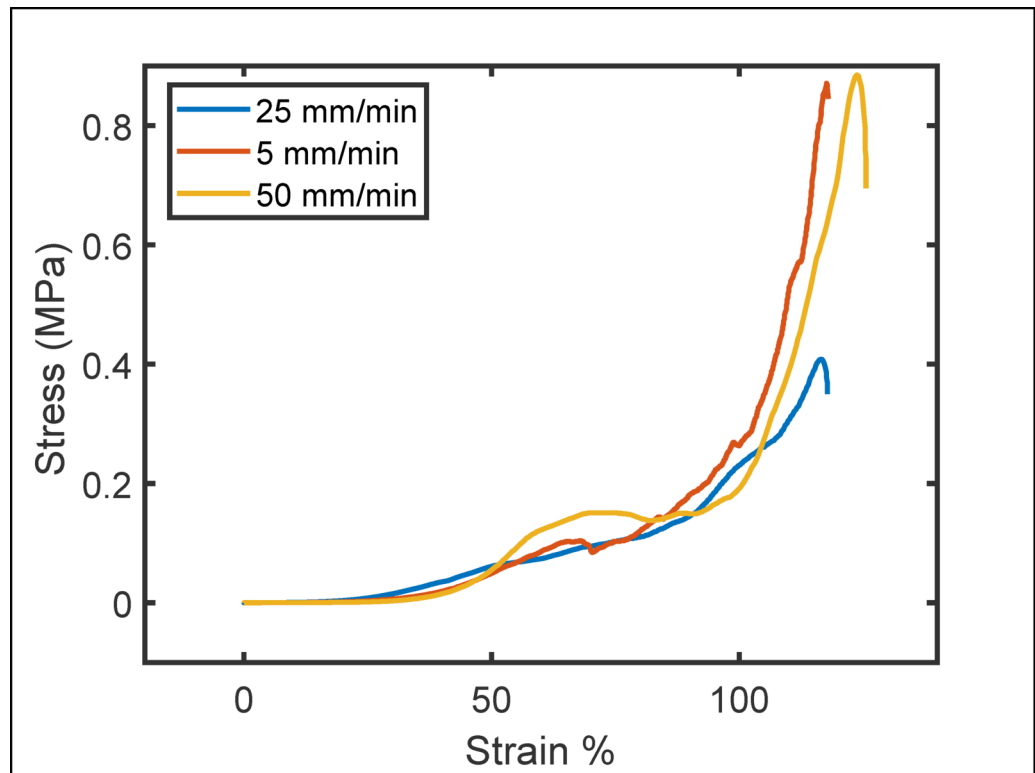


Fig. 2. Compressive stress vs. strain for the cortex region.

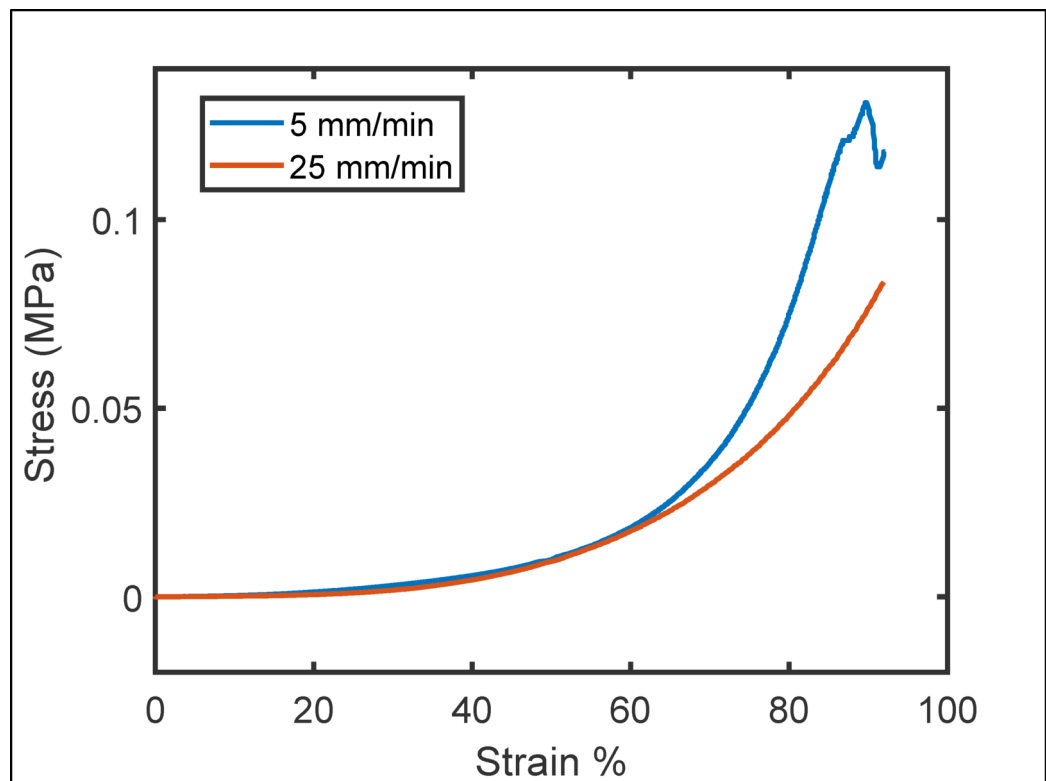


Fig. 3. Compressive stress vs. strain for the medulla region.



Fig. 4. Tissue preparation for compression test/ Zwick/Roell Z050 Universal Testing Machine.

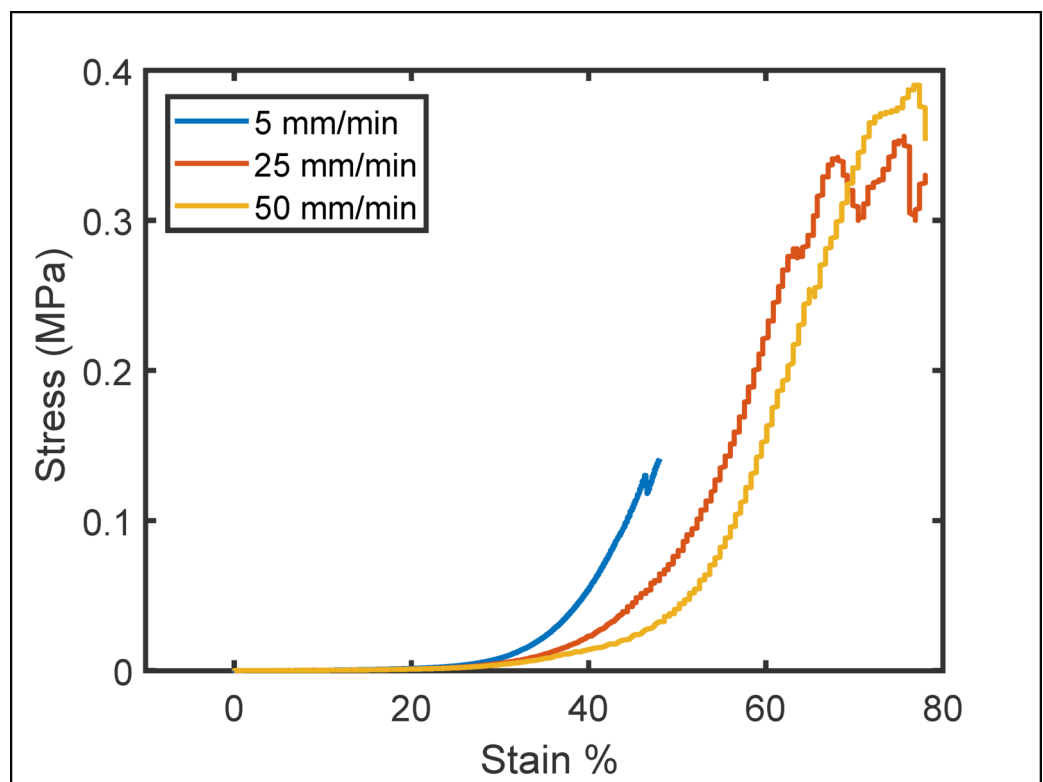


Fig. 5. Compressive stress vs. strain for the entire kidney.

Figure 6 shows the values of stress versus strain rates. Considering the non-linearity of the stress and strain rate relationship, it can be concluded that the viscous property of the material is also non-linear specially at high strain levels. Equation 1 presents the stress as a function of the strain rate.

$$\sigma = \eta \dot{\epsilon} \tag{1}$$

Where $\dot{\epsilon}$ is strain rate, and σ is stress. The viscosity, η , which is defined as the ratio of stress to strain rate is a nonlinear coefficient in this tissue.

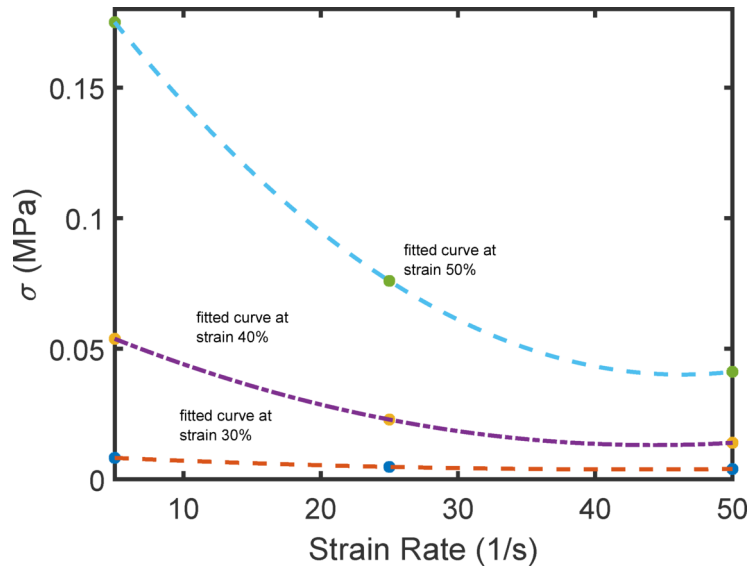


Fig. 6. Stress versus strain rate for the entire organ, dots are experimental data.

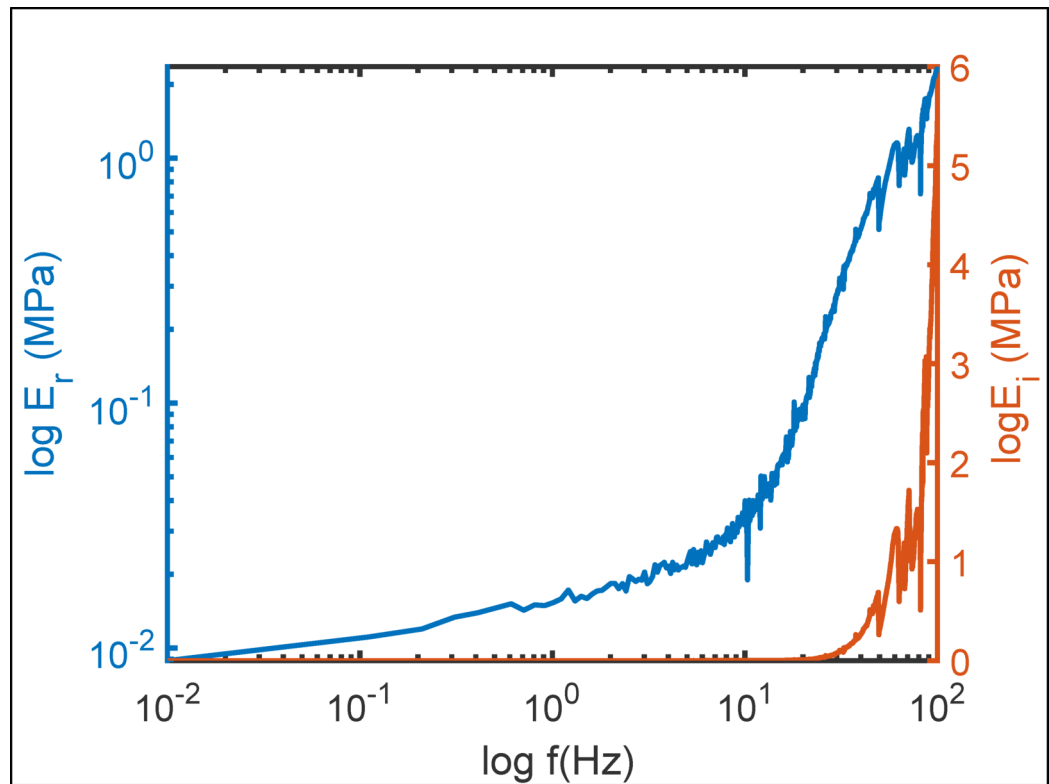


Fig. 7. Real and imaginary part of elastic modulus vs. frequency for the cortex region in Extensive DMA test.

DMA test

Dynamic mechanical analysis (DMA-Mettler Toledo, Switzerland) was performed in extension mode to evaluate the frequency-dependent viscoelastic properties of kidney tissue. The samples were prepared following the protocol described in Section “Mechanical compressive test”. Figures 7 and 8 illustrate the real and imaginary parts of the elastic modulus and tan delta. The test conditions are summarized in Table 1.

According to Figs. 7 and 8 storage and loss modulus and Tan δ coefficient increase with increasing frequency. There is not any extremum in the range of measurement frequency. As the frequency increases, the modulus also

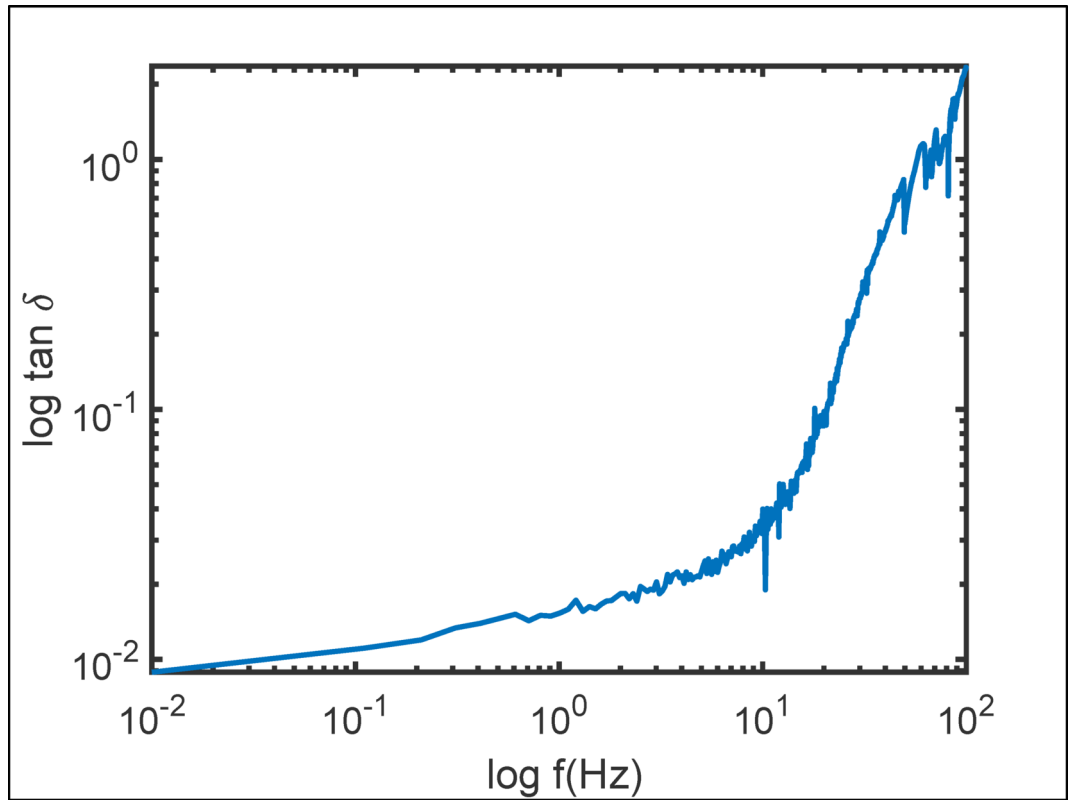


Fig. 8. Tan δ vs. frequency for the cortex region in Extensive DMA test.

Temperature	Dimension	mode	Region	Frequency range
20 °C	Length = 10 mm Width = 8.5 mm Thickness = 2.8 mm	Extension	Cortex	0.01–100 Hz

Table 1. The conditions of the DMA test.

increases, resulting in a stiffer material. This phenomenon resembles the strain rate hardening effect. Previously, these values were reported as 5 to 10 kPa for human kidney²⁴.

Dynamic shear rheometric test

Experimental tests and data analysis are conducted using a rheometer (MRC300, Anton Paar) equipped with custom-made 8 mm diameter circular plates as shown in Fig. 9. In a typical experiment, a sinusoidal deformation is applied to the top plate while the bottom plate remains stationary. Fresh ovine kidney samples were used for this test, collected and handled according to the procedure described in Section “Mechanical compressive test”. A time-dependent shear strain is applied to the sample. The applied stress to the sample calculated using the measured torque. Tests collected four physical values that describe the relationship between strain and stress in particular. These values include the complex modulus (G^*), storage modulus (G'), loss modulus (G''), and phase angle (δ), each of which provides insight into the viscoelastic properties of the material. The storage modulus (G') represents the ability to store energy elastically and resist shear deformations, while the loss modulus (G'') quantifies the ability to dissipate energy through shear deformations. The phase angle (δ) characterizes the viscoelastic nature of a material, reflecting the ratio of the viscous to elastic modulus, commonly expressed as the tangent of δ ($\tan \delta$). Materials which have $\tan \delta > 1$ exhibit predominantly viscous behavior, like fluids, whereas materials with $\tan \delta < 1$ demonstrate greater elasticity, behaving more like solids^{25–27}. These parameters are defined as follows:

$$\tau = G' \gamma_0 \sin(\omega t) + i G'' \gamma_0 \sin(\omega t) \tag{2}$$

$$G^* = G' + i G'' \tag{3}$$

$$|G^*| = \sqrt{|G'|^2 + |G''|^2} \tag{4}$$

$$\tan(\delta) = \frac{G''}{G'} \tag{5}$$

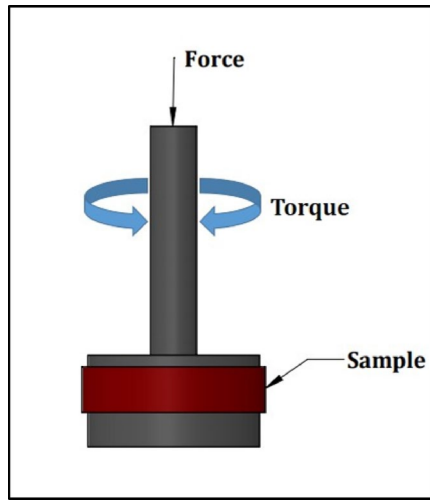


Fig. 9. Scheme of the rheometer used for the tests.



Fig. 10. Samples preparation for rheology tests.

where γ_0 represents the strain, $\omega = 2\pi f$, with f being the frequency of the strain oscillation, t representing time, and i as the imaginary unit.

Shear stress (τ) is calculated using the torque (M) and the plate radius (R) according to the following equation²⁸:

$$\tau = \frac{2M}{\pi R^3} \tag{6}$$

The shear strain amplitude (γ_0) is determined based on the angular displacement (ϕ_0) and the material thickness (h) using the following relation²⁸:

$$\gamma_0 = \frac{\phi_0 R}{h} \tag{7}$$

Figure 10 shows samples for rheology tests.

In order to identify any possible linear region, at a constant frequency of 1 Hz by altering the strain value, the obtained values of G' and G'' can be observed in Fig. 11. This test was conducted at a temperature of 4 degrees centigrade. using a sample with a diameter of 8 mm and a thickness of 1.5 mm taken from the cortex area. As depicted in Fig. 11, there is no region where the values of G' and G'' are completely independent of the strain, indicating that the material's viscoelastic behavior is non-linear.

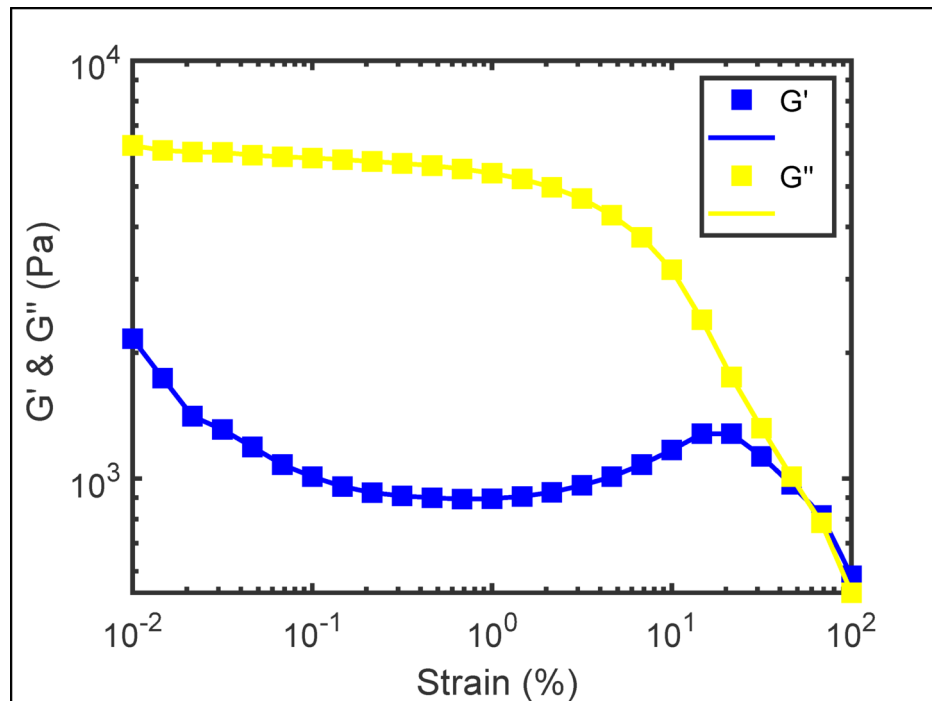


Fig. 11. G' and G'' vs. strain for the cortex region at the constant frequency of 1 Hz.

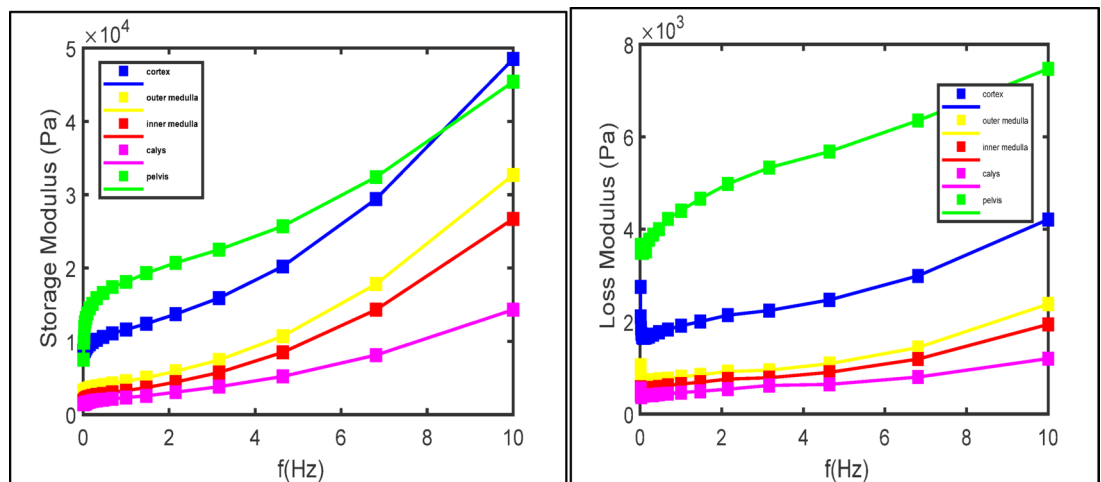


Fig. 12. G' and G'' versus frequency for different regions at the strain of 0.5%.

In the next test, with a frequency range from 0.01 Hz to 10 Hz, the loss, storage modulus, and tan delta values were measured for different areas of the sheep's kidney, and shown in Figs. 12 and 13. The storage modulus increases with increasing frequency. This test was conducted at a temperature of 20 degrees using a sample with a diameter of 8 mm and a thickness of 1.5 mm taken from different regions. To ensure optimal contact between the tissue sample and the rheometer plates, a pre-compressive normal force was applied prior to experiments. The mean normal force measured at the onset of testing was 0.074 ± 0.033 N. This force was carefully chosen to preserve the integrity of the sample while minimizing excessive deformation and slippage during the tests.

In terms of viscoelastic behavior, the ratio of viscous to elastic response varies across different frequencies. As shown in Fig. 13, at higher frequencies, the material exhibits predominantly elastic behavior, whereas at lower frequencies, it demonstrates a more viscous response. This characteristic highlights the nonlinear viscoelastic nature of the kidney tissue. The increase in loss modulus (G'') with frequency is due to the enhanced energy dissipation at higher deformation rates. As frequency increases, molecular rearrangement becomes more restricted, leading to greater internal friction and higher energy loss. This results in an increase in G'' , reflecting the material's ability to dissipate more energy under rapid loading conditions.

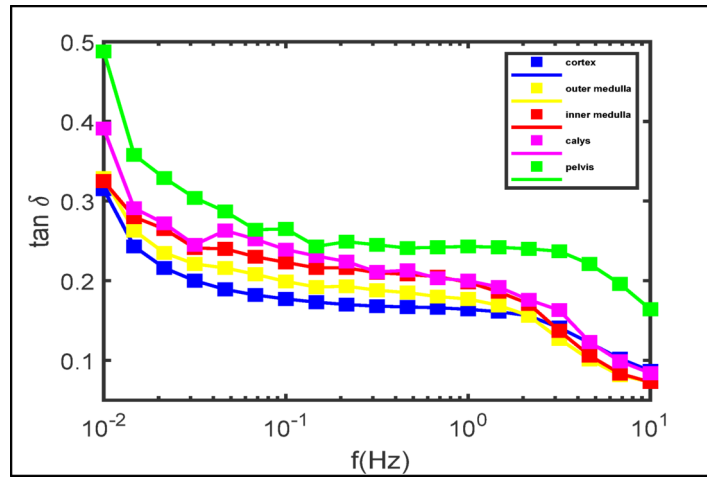


Fig. 13. Tan delta versus frequency for different regions at the strain of 0.5%.

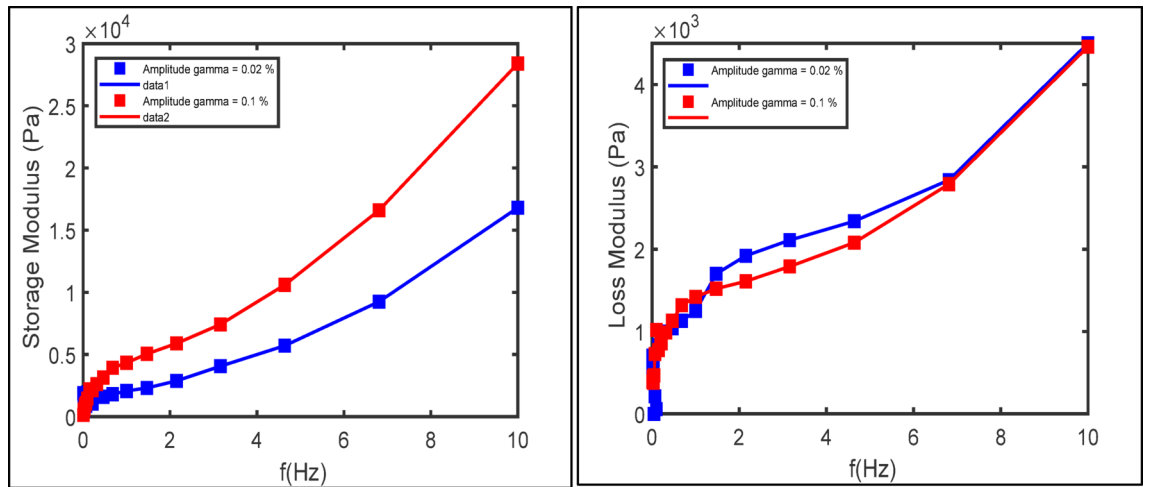


Fig. 14. G' and G'' versus frequency at different strain levels for the cortex region.

To ensure the accuracy of the results, a frequency sweep test was conducted on different strain levels in the cortex area. The results are depicted in Fig. 14.

Receptance FRF of the kidney

The mechanical frequency response test is a method used to determine the dynamic characteristics of a mechanical system. This test involves applying a known force to a system and measuring the resulting displacement. The Frequency Response Function (FRF) is defined as the ratio of the output displacement $X(\omega)$ to the input force $F(\omega)$ in the frequency domain according to Eq. 8. The relationship between the applied force and the resulting displacement provides insights into the system’s stiffness, damping and natural frequencies. In this paper, this method is used to understand the dynamic behavior of the entire organ. The test setup and its schematic are shown in Figs. 15 and 16.

$$H(\omega) = \frac{X(\omega)}{F(\omega)} \tag{8}$$

Ovine kidneys ($N=9$) were excised from sheep at a Slaughterhouse on the same day based on the procedure described in Section “Mechanical compressive test” and placed in the test setup. The data illustrating the amplitude and phase of the receptance FRF is presented in Fig. 17. As depicted in this figure, the amplitude reaches its maximum at the frequency about 3 Hz. The phase of the system changes from zero to minus 90 and then to minus 180 degrees which are indicative patterns of resonance in the response of a second-order mechanical system, which is clearly discernible in this diagram. This experiment is replicated several times to validate the results using different sheep kidneys.

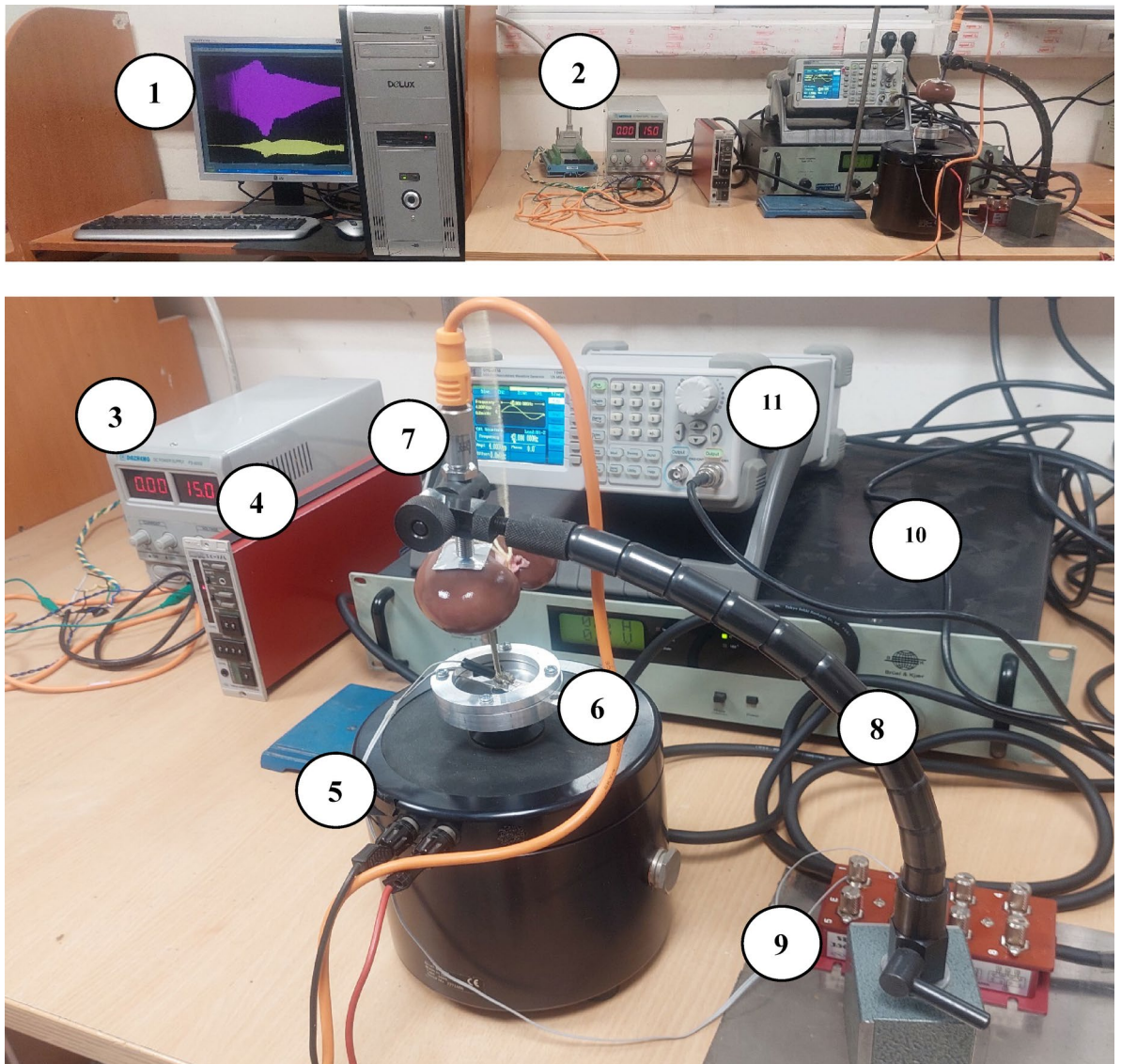


Fig. 15. Mechanical frequency response test setup: 1) PC, 2) Data acquisition card (Advantech 1716 DAQ Card), 3) DC power supply, 4) strain meter, 5) Shaker (B&K model 4809 Made in Denmark, 6) force sensor, 7) displacement sensor ((DW-AD-509-M8-393, Contrinex co.), 8) fixture, 9) Wheatstone bridge box, 10) shaker's amplifier, 11) Function generator (model G305 Made in Japan).

Theoretical model of the system

According to the results of the experimental tests, the system shows a resonance at the frequency about 3 Hz. Since the mechanical system contains mass, stiffness and damping components, a second order transfer function in Laplace space have been proposed to explain its behavior around the resonant frequency.

$$\frac{X(s)}{F(s)} = \frac{G}{ms^2 + cs + k} \quad (9)$$

Which m , c , k and G are equivalent mass, damping, stiffness and the gain of the mechanical system. After substitution of appropriate parameters in the model, Fig. 18 shows the comparison of the model and experimental results.

The values of m , c , k and G in the model are 0.1 kg, 2.2 N. s/m, 60 N/m and 0.39 respectively. As mention in the experimental tests section, the mechanical properties of each region of a kidney are different, but according to the result of the vibration test of the kidney, it is possible to consider an equivalent stiffness of the kidney around the resonant frequency. A FEM model of a kidney which contains all the material properties of a kidney's different regions can predict dynamic mechanical response of the kidney at different frequencies.

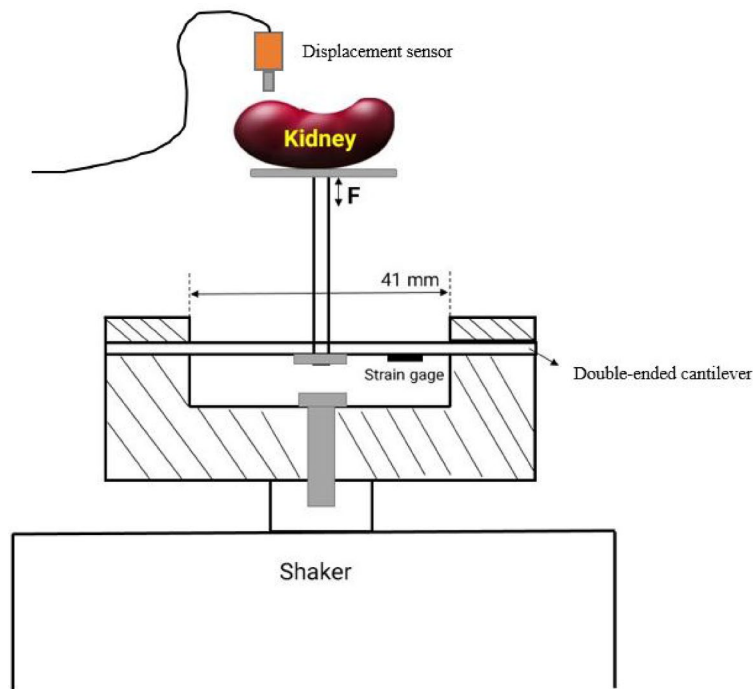


Fig. 16. Schematic of the FRF test.

Numerical modal analysis

In this section, an eigenfrequency analysis of a kidney model is conducted using COMSOL Multiphysics version 6.2. The kidney dimensions are approximately 98 mm × 60 mm × 38 mm, capturing the distinct anatomical regions of a normal kidney. The simulations are performed on a system with an 8-core processor operating at 3 GHz and 32 GB of RAM. Three distinct materials are defined to represent different regions of the kidney: Material 1, assigned to the cortex region, have Young's modulus of 1 kPa, a Poisson's ratio of 0.4, and a density of 1050 kg/m³; Material 2, representing the medulla region, shared the same mechanical properties as Material 1; and Material 3, representing the inner kidney parts, was defined with Young's modulus of 1 kPa, a Poisson's ratio of 0.4, and a slightly lower density of 1030 kg/m³. The maximum strain of the kidney in this analysis is assumed to be less than 5%. Therefore, the Young's modulus of the regions is calculated from the results of a compression test at approximately 5% strain. A normal mesh with free tetrahedral elements was used to ensure an accurate representation of the geometry.

The analysis determined that the first Eigen frequency of the kidney model is approximately 3.3 Hz. This is while, the experimental FRF test demonstrated resonance at 3 Hz, confirming convergence between the experimental and simulation results.

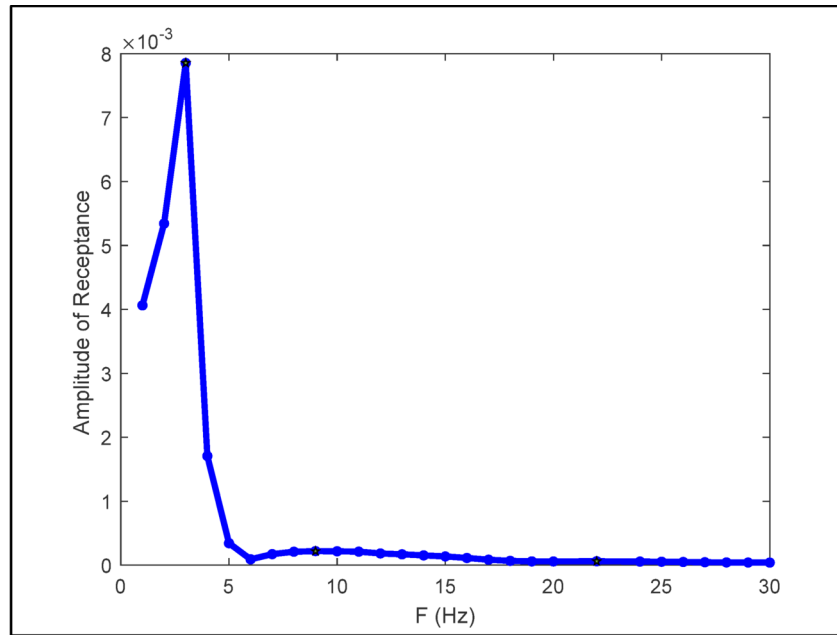
Figure 19 shows the simulated kidney and the results of numerical modal analysis in COMSOL software.

Result

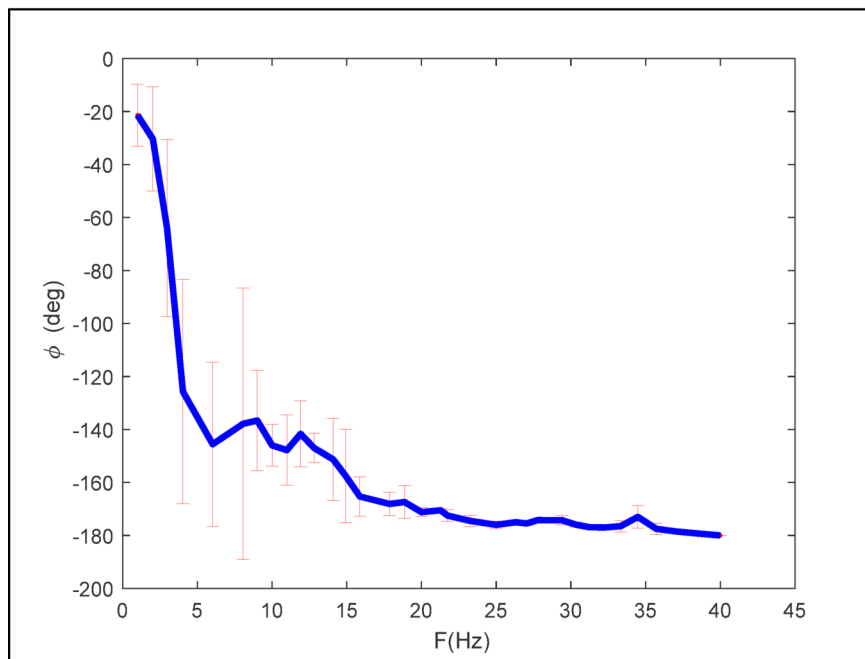
In this study, the resonant patterns in the mechanical properties of different parts of the sheep's kidney and the frequency behavior of the entire organ were examined. According to the experimental results, no resonant behavior was observed in mechanical properties such as storage modulus, loss modulus, and tan delta in tensile and shear modes in the frequency range below 10 Hz. However, the kidney vibration tests data revealed that the entire organ has a resonant frequency around 3 Hz. As shown in Table 2, the descriptive statistics of the resonant frequencies provide an overview of the central tendencies and variability within the data.

Discussion

Using a second-order analytical model, the equivalent mass, stiffness, and damping values of the kidney at this resonant frequency were obtained. Any changes in the material properties of the kidney due to disease or decay processes can affect its stiffness and damping, leading to changes in its natural resonant frequency. These findings can serve as a diagnostic index for kidney health. The results of the numerical modal analysis confirmed the existence of a resonant frequency near 3 Hz. The FRF tests results reveal several key observations about the kidney samples. Notably, there is a sharp drop in the amplitude at higher frequencies, which is typical for soft biological tissues where damping effectively absorbs these higher-frequency vibrations. All samples, exhibit localized peaks that may result from the resonance effect or variations in tissue stiffness. Since these peaks are consistent across all samples, they may indicate the natural frequency of kidneys.



(a)

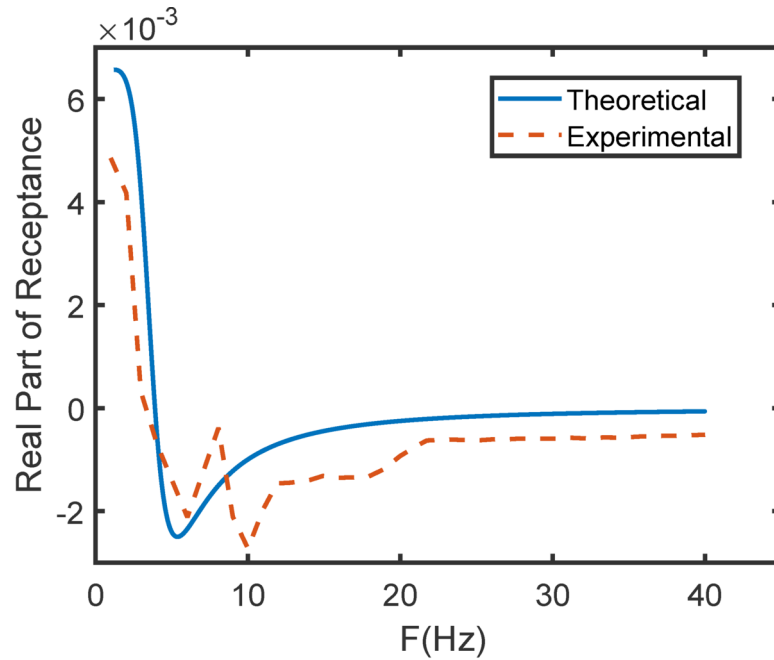


(b)

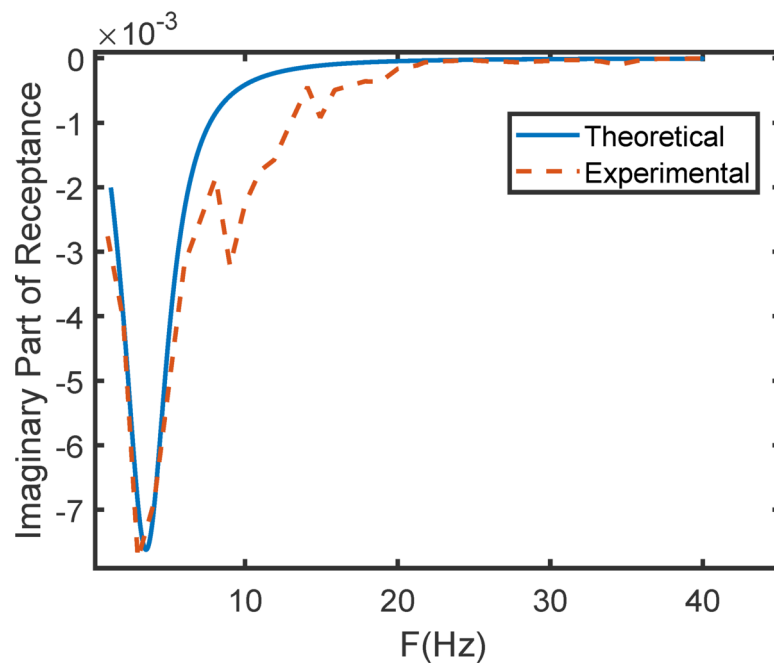
Fig. 17. (a) Amplitude, (b) phase of the receptance FRF.

To ensure that the observed changes in mechanical properties with frequency were due to the viscoelastic nature of the tissue rather than alterations in microstructural arrangements, histological analysis was performed after mechanical testing. Figure 20 shows the results of histological analysis of the kidney tissue.

Kidney tissue sections (4 μm thick) were stained with hematoxylin and eosin (H&E) and examined under a light microscope at with the magnification factor of 400 in at least 10 randomly selected, non-overlapping fields. The histological assessment revealed that glomerular size remained within the normal range, although a slight increase in Bowman's capsule space was noted. Most tubules remained intact with open lumens, and while nuclear condensation and a slight decrease in cellular diameter were observed, no significant vacuolization was detected. These findings suggest that the applied mechanical tests did not induce substantial structural damage



(a)



(b)

Fig. 18. Comparison of the theoretical and experimental real and imaginary parts of the receptance FRF.

to the tissue, supporting the assumption that the frequency-dependent mechanical response primarily reflects the viscoelastic behavior of the renal tissue rather than microstructural deterioration.

Conclusion

This paper presents an experimental investigation into the mechanical properties of ovine renal tissue. The study aims to explore resonance patterns in the tissue's mechanical behavior at low frequencies. Utilizing a universal tensile/compression testing machine, the stress-strain behavior of the tissue under compression was analyzed, highlighting its non-linear viscoelastic characteristics. Dynamic Mechanical Analysis (DMA) and a dynamic shear rheometer were employed to assess key mechanical properties, including storage modulus and loss

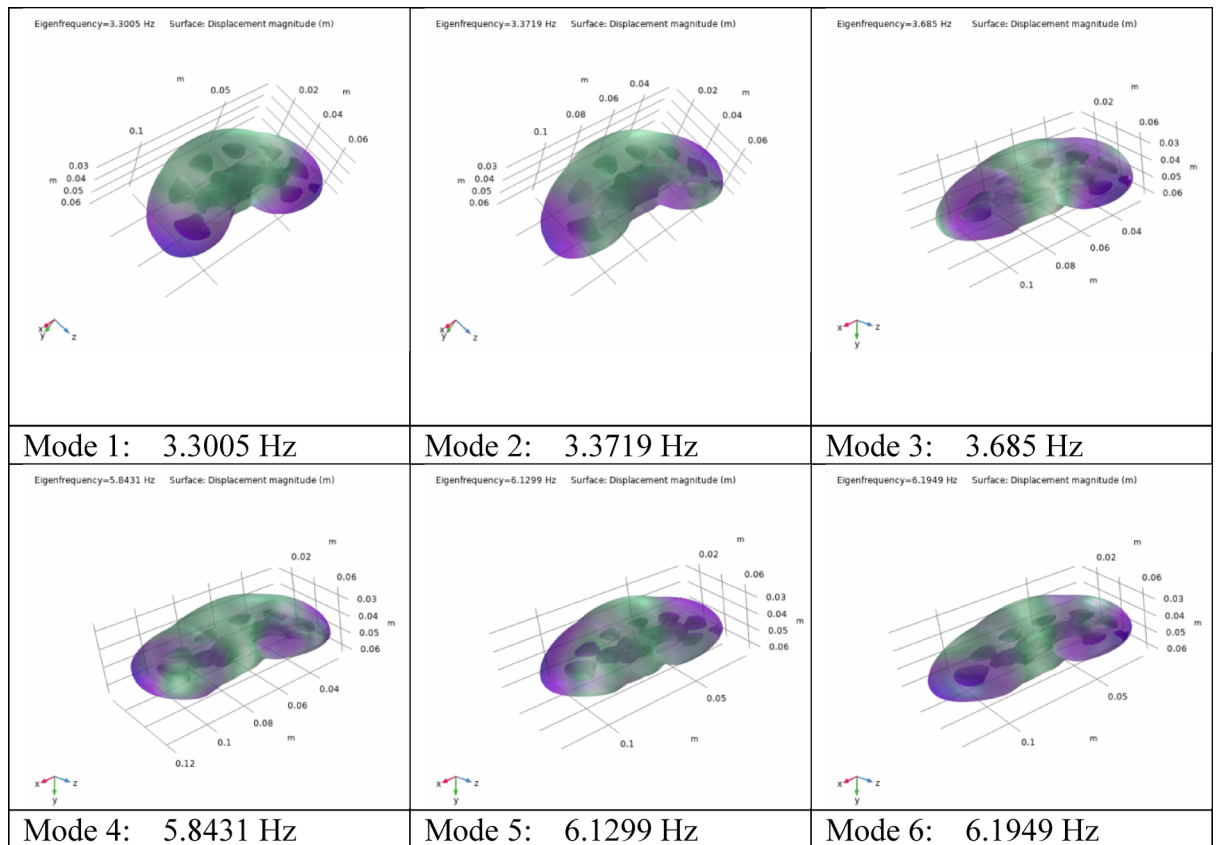


Fig. 19. (a) simulated kidney (b) the results of numerical modal analysis in COMSOL software.

Statistic	Mean	Median	Standard deviation	Min	Max
Frequencies (Hz)	3.3	3	0.8	2	5

Table 2. Descriptive statistics for the resonant frequencies of fresh kidneys.

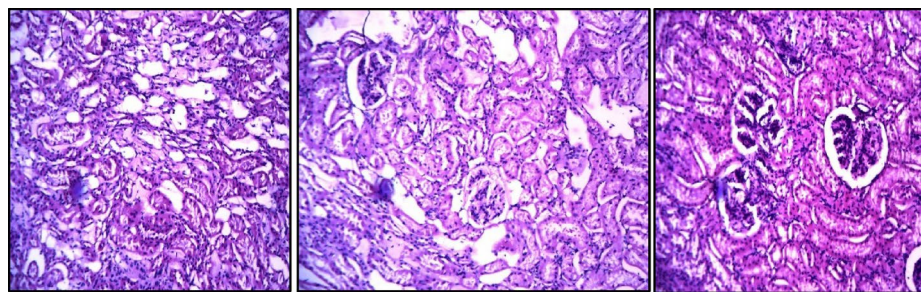


Fig. 20. Histological analysis of renal tissue after mechanical testing (H&E Staining, 400× Magnification).

modulus, across various frequencies. Vibration tests were conducted on the kidney using a shaker to examine the receptance Frequency Response Function (FRF) of the organ within the specified frequency range. The results of the vibration tests indicated a resonant frequency for the entire organ at approximately 3 Hz. To further validate these findings, a Finite Element Model (FEM) of the kidney was developed, and numerical modal analysis confirmed the presence of a resonance frequency near 3 Hz. These results suggest that variations in the material properties of the kidney can lead to changes in its natural resonant frequency, indicating that resonant frequency may serve as a valuable index for diagnosing kidney health.

Data availability

The datasets used and/or analyzed during the current study available from the corresponding author on reasonable request.

Received: 11 December 2024; Accepted: 5 May 2025

Published online: 12 May 2025

References

- Guimarães, C. F., Gasperini, L., Marques, A. P. & Reis, R. L. The stiffness of living tissues and its implications for tissue engineering. *Nat. Rev. Mater.* **5**, 351–370 (2020).
- Golahmadi, A. K., Khan, D. Z., Mylonas, G. P. & Marcus, H. J. Tool-tissue forces in surgery: A systematic review. *Ann. Med. Surg.* **65**, 102268 (2012). <https://doi.org/10.1016/j.amsu.2021.102268> (2021).
- Lim, Y. J., Deo, D., Singh, T. P., Jones, D. B. & De, S. In situ measurement and modeling of Biomechanical response of human cadaveric soft tissues for physics-based surgical simulation. *Surg. Endosc.* **23** (6), 1298–1307. <https://doi.org/10.1007/s00464-008-0154-z> (2009).
- Eroles, M. & Rico, F. Advances in mechanical biomarkers. *J. Mol. Recognit. JMR.* **36** (8), e3022. <https://doi.org/10.1002/jmr.3022> (2023).
- Warden, S. J. et al. Fracture discrimination capability of ulnar flexural rigidity measured via cortical bone mechanics technology: Study protocol for the STRONGER study. *JBMR Plus.* **8** (1), ziad002. <https://doi.org/10.1093/jbmrpl/ziad002> (2024).
- Chan, D. D. et al. In vivo articular cartilage deformation: Noninvasive quantification of intratissue strain during joint contact in the human knee. *Sci. Rep.* **6**, 19220. <https://doi.org/10.1038/srep19220> (2016).
- Singh, G., Gupta, V. & Chanda, A. Artificial skin with varying Biomechanical properties. *Mater. Today Proc.* **62**, 3162–3166. <https://doi.org/10.1016/j.matpr.2022.03.433> (2022).
- Mulk, M., Islam, K. N. & Biswas, M. H. A. Modeling and numerical analysis for mechanical characterization of soft tissue mechanism applying inverse finite element technique. *Front. Appl. Math. Stat.* **9** (2023). <https://doi.org/10.3389/fams.2023.1064130>
- Fotiadis, D. I., Sakellarios, A. I. & Potsika, V. T. Computational modeling at tissue level (pp. 117–152). (2023). <https://doi.org/10.1002/9781119819028.ch5>
- Guo, J. et al. Piezoresistivity modeling of soft tissue electrical-mechanical properties: A validation study. *Proc. Inst. Mech. Eng. Part. H J. Eng. Med.* **237** (8), 936–945. <https://doi.org/10.1177/09544119231183545> (2023).
- Tac, V., Sree, V. D., Rausch, M. K. & Tepole, A. B. Data-driven modeling of the mechanical behavior of anisotropic soft biological tissue. *Eng. Comput.* **38** (5), 4167–4182. <https://doi.org/10.1007/s00366-022-01733-3> (2022).
- Chatelin, S. et al. In vivo liver tissue mechanical properties by transient elastography: Comparison with dynamic mechanical analysis. *Biorheology* **48** (2), 75–88. <https://doi.org/10.3233/BIR-2011-0584> (2011).
- Griffin, M., Premakumar, Y., Seifalian, A., Butler, P. E. & Szarko, M. Biomechanical characterization of human soft tissues using indentation and tensile testing. *J. Visual. Exp. JoVE.* (118), 54872. <https://doi.org/10.3791/54872> (2016).
- Barak, M. M. & Black, M. A. A novel use of 3D printing model demonstrates the effects of deteriorated trabecular bone structure on bone stiffness and strength. *J. Mech. Behav. Biomed. Mater./J. Mech. Behav. Biomed. Mater.* **78**, 455–464. <https://doi.org/10.1016/j.jmbbm.2017.12.010> (2018).
- Vappou, J. et al. Magnetic resonance elastography compared with rotational rheometry for in vitro brain tissue viscoelasticity measurement. *Magn. Reson. Mater. Phys. Biol. Med.* **20** (5–6), 273–278. <https://doi.org/10.1007/s10334-007-0098-7> (2007).
- Lin, H. et al. Viscoelastic properties of normal rat liver measured by ultrasound elastography: Comparison with oscillatory rheometry. *Biorheology* **53** (5–6), 193–207. <https://doi.org/10.3233/bir-16091> (2017).
- Barbe, K., Ford, C., Bonn, K. & Gilbert, J. Non-parametric frequency response function tissue modeling in bipolar electrosurgery. (2015). <https://doi.org/10.1109/embc.2015.7319764>
- Bediz, B., Özgüven, H. N. & Korkusuz, F. Vibration measurements predict the mechanical properties of human tibia. *Clin. Biomech. Elsevier Ltd.* **25** (4), 365–371 (2010).
- Johnson, B., Campbell, S. & Campbell-Kyureghyan, N. Characterizing the material properties of the kidney and liver in unconfined compression and probing protocols with special reference to varying strain rate. *Biomechanics* **1** (2), 264–280. <https://doi.org/10.3390/biomechanics1020022> (2021).
- Felix-Mihai, M., Bob, F., Grosu, I. D., Schiller, A. & Petrica, L. #4624 Viscoelasticity measurement- a new ultrasound-based elastography method in the assessment of the kidney. *Nephrol. Dialysis Transpl.* **38** (Supplement_1). https://doi.org/10.1093/ndt/gfad063c_4624 (2023).
- Yokoyama, K. A. et al. In vivo VisR measurements of viscoelasticity and viscoelastic anisotropy in human allografted kidneys differentiate interstitial fibrosis and graft rejection. *2022 IEEE Int. Ultrason. Symp. (IUS)*. <https://doi.org/10.1109/ius54386.2022.9958358> (2022).
- Akilesh, S. Normal kidney function and structure. In Elsevier eBooks (pp. 2716–2733). (2014). <https://doi.org/10.1016/b978-0-12-386456-7.05402-2>
- Johnson, R. J., Floege, J. & Tonelli, M. *Comprehensive Clinical Nephrology - E-Book* (Elsevier Health Sciences, 2023).
- Handorf, A. M., Zhou, Y., Halanski, M. A. & Li, W. Tissue stiffness dictates development, homeostasis, and disease progression. *Organogenesis* **11** (1), 1–15. <https://doi.org/10.1080/15476278.2015.1019687> (2015).
- McCarthy, A. D., Soares, D. J., Chandawarkar, A., El-Banna, R. & Hagedorn, N. Dilutional rheology of radiess: Implications for regeneration and vascular safety. *J. Cosmet. Dermatol.* **23** (6), 1973–1984. <https://doi.org/10.1111/jocd.16216> (2024).
- van der Sman, R. G. M., Renzetti, S. & Tian, B. Rheology of edible soft glassy materials. *Food Hydrocoll.* **149**, 109586 (2024).
- Perni, S. & Prokopovich, P. Rheometer enabled study of cartilage frequency-dependent properties. *Sci. Rep.* **10**, 20696. <https://doi.org/10.1038/s41598-020-77758-9> (2020).
- Laun, M. et al. Guidelines for checking performance and verifying accuracy of rotational rheometers: viscosity measurements in steady and oscillatory shear (iupac technical report). *Pure Appl Chem.* **86**, 1945–68. (2014).

Author contributions

Mohammad Reza Karafi: He supervised the research, validated the experimental results, provided the ideas for the tests and analysis, and revised the paper. Faezeh Azimi Pirsoltan: She conducted the experiments and analysis, and wrote the first draft of the paper.

Funding

The authors did not receive support from any organization for the submitted work. No funding was received to assist with the preparation of this manuscript. No funding was received for conducting this study.

Declarations

Competing interests

The authors declare no competing interests.

Additional information

Supplementary Information The online version contains supplementary material available at <https://doi.org/10.1038/s41598-025-01302-w>.

Correspondence and requests for materials should be addressed to M.R.K.

Reprints and permissions information is available at www.nature.com/reprints.

Publisher's note Springer Nature remains neutral with regard to jurisdictional claims in published maps and institutional affiliations.

Open Access This article is licensed under a Creative Commons Attribution-NonCommercial-NoDerivatives 4.0 International License, which permits any non-commercial use, sharing, distribution and reproduction in any medium or format, as long as you give appropriate credit to the original author(s) and the source, provide a link to the Creative Commons licence, and indicate if you modified the licensed material. You do not have permission under this licence to share adapted material derived from this article or parts of it. The images or other third party material in this article are included in the article's Creative Commons licence, unless indicated otherwise in a credit line to the material. If material is not included in the article's Creative Commons licence and your intended use is not permitted by statutory regulation or exceeds the permitted use, you will need to obtain permission directly from the copyright holder. To view a copy of this licence, visit <http://creativecommons.org/licenses/by-nc-nd/4.0/>.

© The Author(s) 2025